Hindawi Publishing Corporation
International Journal of Antennas and Propagation
Volume 2015, Article ID 438962, 10 pages
http://dx.doi.org/10.1155/2015/438962

Research Article

Culture Medium Geometry: The Dominant Factor Affecting In Vitro RF Exposure Dosimetry

Alessandra Paffi,[1] Francesca Apollonio,[1] Micaela Liberti,[1] Asher Sheppard,[2] Giorgi Bit-Babik,[3] and Quirino Balzano[4]

[1]*Sapienza University of Rome, 00184 Rome, Italy*
[2]*Asher Sheppard Consulting, 4960 Hoen Avenue, Santa Rosa, CA 95405, USA*
[3]*Motorola Solutions, Inc., Plantation, FL 33322, USA*
[4]*University of Maryland, Rm 2134, Kim Building, College Park, MD 20742, USA*

Correspondence should be addressed to Quirino Balzano; qbalzano@umd.edu

Received 13 November 2014; Accepted 30 December 2014

Academic Editor: Diego Caratelli

Copyright © 2015 Alessandra Paffi et al. This is an open access article distributed under the Creative Commons Attribution License, which permits unrestricted use, distribution, and reproduction in any medium, provided the original work is properly cited.

Biological experiments that expose living cells or tissues to RF energy must have an aqueous medium to provide essential water, ions, nutrients, and growth factors. However, as we show here, the medium inherently functions as a receiving antenna that conveys RF energy to the biological entity in a manner entirely determined by exposure vessel geometry, orientation to the incident RF flux, frequency, and dielectric properties of the medium. We show for two common experimental arrangements that basic antenna theory can predict electromagnetic energy patterns that agree well with those otherwise obtained by computationally intensive methods that require specialized resources.

1. Introduction

Over the last half century researchers have exposed cell preparations to RF electromagnetic (EM) energy to explore mechanisms of interaction of living cells with EM fields [1]. Early experiments frequently were conducted by exposing biological preparations to an incident EM wave of given power density. However, the pattern of the RF field exposure of cells within the medium was not investigated for lack of analytical tools, leaving investigators with little knowledge of the distribution of energy absorbed by the cells under test. Unless there is a clear understanding of the physics of EM fields, it is possible to miss the overall character of RF absorption by a biological preparation.

The last two decades [2–4] have seen substantial advancements in theoretical and experimental dosimetry. Minimal requirements for exposure systems have been established [5] and are now widely accepted. The detailed distribution of absorbed energy inside an exposure vessel requires computer algorithms that accurately model the fine details of exposure systems and exposed samples. One such numerical method is the finite difference time domain (FDTD) algorithm based on numerical procedures to solve the EM problem within a region of space [6].

The FDTD method performs a point-by-point evaluation of the EM fields whereas the analytical approach proceeds from the first principle, Faraday's law, in describing the interaction between the fields and the medium. Consequently, the analytic models reveal the physical events underlying the computational results.

This paper aims to show that the culture medium of a biological preparation not only supports cell metabolism but also conveys the EM energy absorbed by the tissues and cells under test, illustrating the usefulness of the concept that the medium is an antenna whose geometric and dielectric properties entirely determine the biologically relevant exposure. The cells themselves have a passive role as absorbers of EM energy from the local environment. Equivalently, the cells can be considered as a distributed load of a dielectric antenna consisting of the medium in which they are embedded. This paper also presents analytical approaches that are simpler than numerical FDTD computations and sufficiently accurate

for fast, preliminary estimation of the SAR in cylindrical vessels containing a biological preparation.

2. Exposure of Preparations in Petri Dishes and Test Tubes

Test tubes, flasks, and dishes of various sizes are the three vessels commonly used for the exposure of cells to RF EM energy. We limit our considerations to Petri dishes of 34 mm inner diameter (ID) and test tubes, both of which have cylindrical (rotational) symmetry. Exposure systems with other vessel geometries can be analyzed by a similar methodology. The simplest (canonical) exposure of a cylindrical structure to a propagating wave can be performed with the direction of propagation either oriented along the axis of the cylinder or orthogonal to it. Axial propagation with incidence from the bottom or the top of the vessel is designated as k^+ and k^-, respectively. Waves with incidence orthogonal to the axis of the cylinder have either the E- or the H-field oriented along the axis. All other exposures are a combination of these four conditions. For stationary waves, there are only three independent geometric exposures: both E- and H-field parallel to the cross section plane and H or E parallel to the axis of the vessel. While all four types of propagating wave exposure have been used in laboratory research [7–10], only the stationary waves with E and H parallel to the cylindrical cross section and the stationary H-field exposure have been employed [11, 12].

3. RF EM Field Propagation in Dielectric Cylinders

We focus our attention on exposures utilizing EM fields in the band 900 MHz–5 GHz, the frequencies most used for cellular communications. Our analyses of the absorption of RF energy by cell preparations in Petri dishes and test tubes treat the medium as if it were a simple cylindrical receiving antenna made of a dissipative dielectric material.

Cylindrical dielectric antennas have been analyzed, designed, and used for more than a century [13–16]. The distribution of RF energy within dielectric cylinders depends strictly on the boundary conditions at their surface. Consequently, the field distribution differs significantly for systems with propagation along the cylindrical axis from others with propagation perpendicular to the axis [15–17]. RF propagation along the axis of a dielectric cylinder is presented in detail in [16], where it is shown that there are discrete modes of propagation. In the case of a plane wave incident normal to the cylindrical surface with the E- or H-field parallel to the cylindrical axis, the resulting internal fields were analyzed by Stratton [17] and Harrington [18]. All incident directions can be treated analytically if the dielectric cylinder is long enough that end effects can be disregarded. While test tubes can support axial wave propagation if the medium depth is a sufficiently large part of the wavelength, this certainly is not the case for Petri dishes, which contain only a few milliliters of medium with a typical depth of 2–4 mm, a small fraction of a wavelength in the band of our interest. Before presenting the infinite cylinder solutions for medium in a Petri dish or test tube, it is necessary to explore the influence on their validity of end effects and deviations from perfect geometric form.

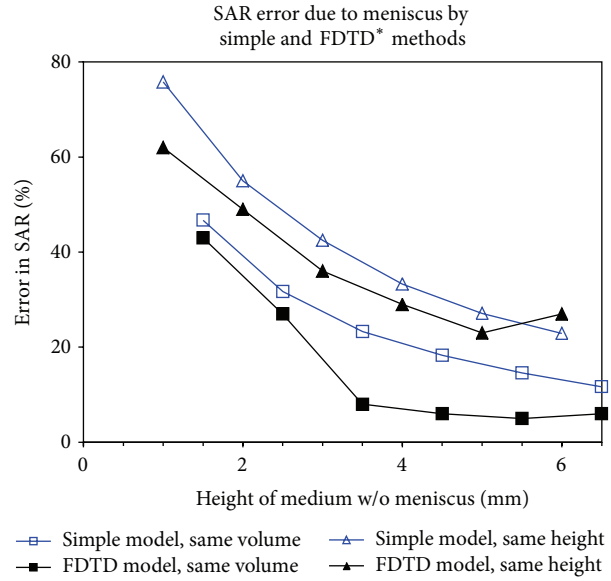

Figure 1: SAR error at the bottom of a 34 mm ID Petri dish.

3.1. Meniscus and Antenna Effect in Petri Dishes, E-Polarization. A concave meniscus is present for all aqueous columns that wet their glass or plastic container. Although a meniscus does not break the cylindrical symmetry of the vessels of interest, it can cause substantial end effects if it contains a significant fraction of the liquid volume. We analyze the meniscus effects treating the liquid medium as an antenna. A meniscus does not affect substantially the internal fields of the medium-antenna for k^+, k^-, or H-polarized waves, but can be a significant factor for E-polarization if the meniscus height is comparable to the liquid depth at the center of the container, as first reported in [4]. The reason is simple: the presence of the meniscus increases substantially the cross sectional area of the medium/antenna that couples with the magnetic flux from the incident H-field as compared to the area of the cross section of the same total liquid volume without a meniscus (Figure 7).

Appendix A presents the detailed analysis of the effect of the meniscus on the average specific absorption rate (SAR) at the bottom of a Petri dish exposed to the peak H-field of a E-polarized stationary wave at 1800 MHz. It is the exposure system investigated in [4] using numerical algorithms. The antenna analysis of Appendix A is simple and direct but does not require the computational resources needed for an FDTD analysis as a hand calculator suffices. The results of neglecting the meniscus effect are shown in Figure 1 for a Petri dish with 34 mm ID. The "same volume" and "same height" labels stand for the case of the dish with the same volume of liquid with or without the meniscus and, alternatively, the same liquid height with or without the meniscus. From Figure 1, it is

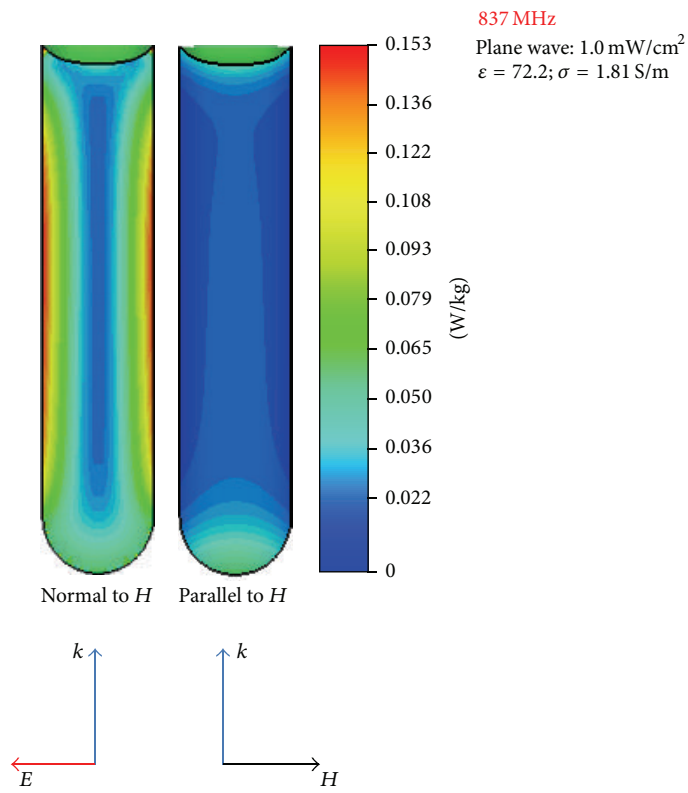

Figure 2: SAR patterns in a liquid medium.

possible to conclude that for Petri dishes of 34 mm ID with 4 mm depth of medium (without counting the meniscus height) the meniscus end effect can be neglected as the SAR error is less than 10%.

3.2. Antenna Effects and Guided Waves in Test Tubes, k^+-Polarization. We analyzed the exposure of biological preparations in test tubes to a 10 W/m^2 plane wave at 837 MHz using CST Microwave Studio [19] and FDTDLab, an independently developed computational suite [20]. Both algorithms yield similar results. The meshing size used to represent the liquid in the computations was 0.3 mm. Figure 2 shows the SAR distribution in the medium. The depth of the biological liquid inside the test tube is $L = 62.7$ mm and the radius is $a = 8.45$ mm. The dielectric characteristics of the medium (permittivity ε_r and conductivity σ) are given in the figure legends. The liquid column behaves as a loop antenna in the plane orthogonal to the magnetic field (Figure 2, left side). Applying Faraday's law to the outermost closed path that can be drawn in the medium, one finds E_{AV}, the average value of the E-field, and SAR_{AV}, the average value of the SAR along the periphery of the cross section normal to the H-field. They are

$$E_{AV} = \omega\mu_0 H \frac{2a \times L - (2 - \pi/2)\, a^2}{2\,(2a + L) + a \times (2\pi - 4)} = 6.21 \text{ V/m},$$
$$\text{SAR}_{AV} = 70 \text{ mW/kg}. \quad (1)$$

The peak SAR can be approximated by applying Lenz's law, according to which minimization of magnetic flux concatenated with the antenna requires that current induction is greater in the two long sides of the loop. The RF currents can be represented roughly by a sinusoid that peaks in the middle of the side. This procedure yields an estimated peak SAR value of $\pi^2/4 \times 70 = 173$ mW/kg, which is about 0.5 dB higher than the peak SAR value from FDTD methods shown in Figure 2. The detailed distribution of the SAR in the medium mass requires the use of numerical methods or a rigorous application of Lenz's law, a lengthy procedure involving variational calculus. In contrast, the very simple antenna model just described gives an acceptable approximation of the peak value of the exposure. The E-field has negligible coupling with the liquid column, only end effects, as expected given the very small dimension of its diameter ($\approx 0.05\,\lambda$) with respect to wavelength.

The approach just described has limitations: the rectangular loop perimeter must be less than a half wavelength and two sides of the loop must be much longer than the other two in order to ignore the currents induced in the short sides.

The physical details of EM energy absorption by a cylindrical liquid mass can be analyzed by varying its height (or depth) from a very small to a substantial fraction of the wavelength. For this purpose, the absorption patterns for various depths of a dielectric liquid exposed to a plane wave at 1.8 GHz were computed. The same computational tools discussed above were used and the incident EM fields again propagated in the direction of the cylindrical axis. The

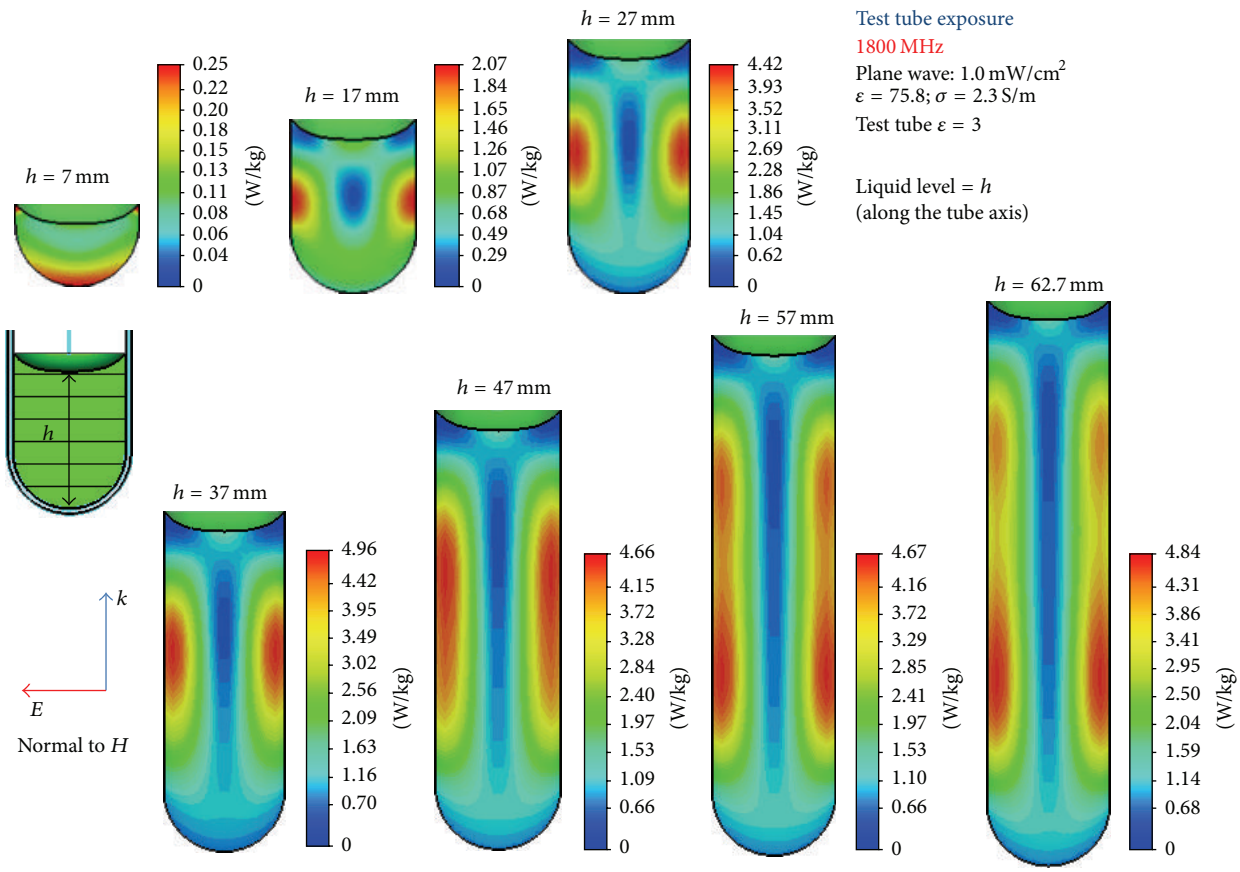

FIGURE 3: SAR patterns in the plane orthogonal to the H-field for various liquid depths with incident 1800 MHz plane wave.

patterns in the planes orthogonal to the H- and E-field are shown in Figures 3 and 4, respectively. One feature is clearly observed comparing Figures 2 and 3: the depth of penetration of the RF energy is much greater at the higher frequency, in agreement with the results reported in [2]. This fact shows that there are modal excitation and wave propagation inside the cylindrical mass. The phenomenon is clearly visible in Figure 4 for the higher liquid columns where end effects do not mask the attenuated propagation of EM fields at the core of the liquid. The theory of the modes in a dielectric rod is found in [16], where the following equation is given for the fundamental TM mode:

$$-\sqrt{\varepsilon_{rc}}\frac{J_1(qa)}{qaJ_0(qa)} + \frac{K_1(pa)}{paK_0(pa)} = 0. \quad (2)$$

In (2), q and p are the radial propagation constants inside and outside the liquid, ε_{rc} is its complex relative dielectric constant, the J's are Bessel functions of the first kind and the K's are modified Bessel functions of the second kind of orders 0 and 1.

The axial propagation constant (β) is given by $\beta^2 = \varepsilon_{rc}(2\pi/\lambda)^2 - p^2$, with λ = free space wavelength.

The following relation also holds: $(pa)^2 + (qa)^2 = (\varepsilon_{rc} - 1)(2\pi a/\lambda)^2$. Equation (2) can be solved using MATLAB [20] and the axial attenuation constant of the fundamental TM mode is found to be $2\pi/\lambda \times 1.51$ per/wavelength [15]. This value matches the axial attenuation of the SAR in the rightmost panel of Figure 4. Computations of the propagation constant of the dielectric cylinder modes can be carried out with readily available mathematical software. If the axial attenuation constants of the modes are not very large, then the simple low frequency approximation of a loop in a constant H-field is not valid because the cylindrical mass behaves like a dielectric waveguide, a device often used as an antenna [21].

3.3. SAR in Petri Dishes, H-Polarization. In our analysis, the medium in the Petri dish is treated as a fluid column of infinite extent in the axial direction. Clearly this is an approximate model of the real situation where the liquid is only a few mm deep. Nonetheless, as we will show below, the model provides useful results at a sufficiently high frequency.

The magnetic field of a plane wave polarized in the direction of the cylindrical axis (z) can be represented in terms of cylindrical functions [17]:

$$H_z^i = H_0 e^{-jkx} = H_0 \sum_{n=-\infty}^{+\infty} j^{-n} J_n(k\rho)\, e^{jn\phi}, \quad (3)$$

where k is the free space propagation constant $k = 2\pi/\lambda$, ρ the radial coordinate of a cylindrical reference system with z as the axis, and J_n denotes a Bessel function of first kind and order n.

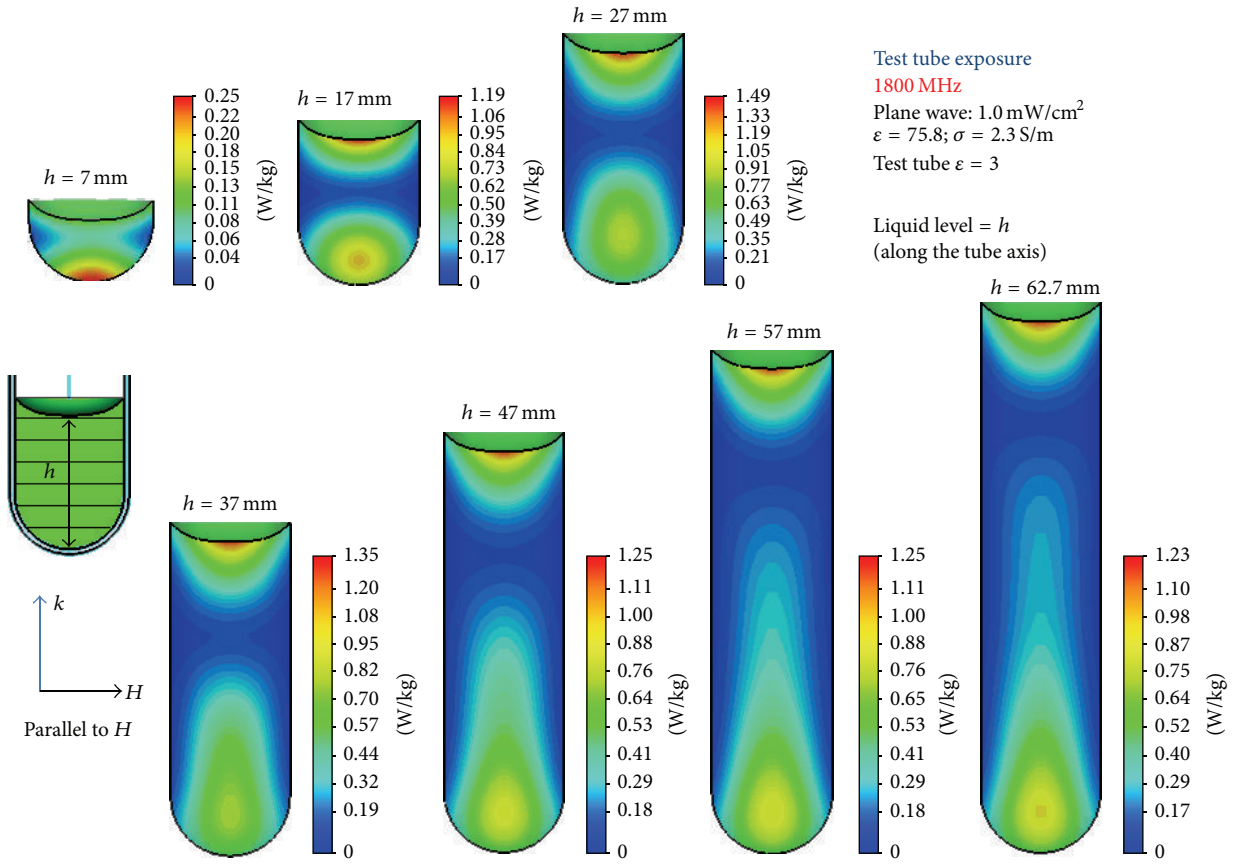

FIGURE 4: SAR patterns in the plane orthogonal to the E-field for various liquid depths with incident 1800 MHz plane wave.

The electric field of the plane wave is found from the equation

$$\begin{aligned}
&\vec{E} = \frac{1}{-j\omega\varepsilon_0}\nabla \times z_0 H_0 e^{-jkx} \text{ which yields:}\\
&E_y^i = \frac{kH_o}{\omega\varepsilon_0}e^{-jkx} = \frac{kH_o}{\omega\varepsilon_0}\sum_{n=-\infty}^{+\infty} j^{-n}J_n(k\rho)\,e^{jn\phi},\\
&E_\phi^i = \frac{kH_o}{\omega\varepsilon_0}\cos\phi \sum_{n=-\infty}^{+\infty} j^{-n}e^{jn\phi}J_n(k\rho)\\
&\quad = j\frac{kH_o}{\omega\varepsilon_0}\sum_{n=-\infty}^{+\infty} j^{-n}e^{jn\phi}J_n'(k\rho),\\
&E_\rho^i = \frac{kH_o}{\omega\varepsilon_0}\sin\phi \sum_{n=-\infty}^{+\infty} j^{-n}J_n(k\rho)\,e^{jn\phi}\\
&\quad = \frac{kH_o}{\omega\varepsilon_0}\sum_{n=-\infty}^{+\infty} j^{-n}e^{jn\phi}n\frac{J_n(k\rho)}{k\rho}.
\end{aligned} \tag{4}$$

In the equation above J_n' denotes the derivative with respect to the argument of the Bessel function of first kind and order n.

The magnetic field H_z^s scattered by an infinite dielectric cylinder can be represented by the infinite series [17]

$$H_z^s = \sum_{n=-\infty}^{+\infty} j^{-n}b_n H_n^{(2)}(k\rho)\,e^{jn\phi}. \tag{5}$$

In (5), $H_n^{(2)}(k\rho)$ is a cylindrical Bessel function of the third kind of order n and b_n is the space harmonic magnetic field amplitude.

The electric field components associated with the scattered magnetic field are given by

$$\begin{aligned}
E_\phi^s &= \frac{1}{j\omega\varepsilon_0}e^{jn\phi}\frac{\partial}{\partial\rho}\sum_{n=-\infty}^{+\infty} j^{-n}b_n H_n^{(2)}(k\rho),\\
E_\rho^s &= \frac{1}{-j\omega\varepsilon_0}\frac{\partial}{\rho\partial\phi}\sum_{n=-\infty}^{+\infty} j^{-n}b_n H_n^{(2)}(k\rho)\,e^{jn\phi}.
\end{aligned} \tag{6}$$

The fields inside the cylinder can be represented as a superposition of TE (with respect to the axial direction) electromagnetic fields [16]. Specifically

$$H_z^c(\rho,\phi) = \sum_{n=-\infty}^{+\infty} a_n \psi_n = \sum_{n=-\infty}^{+\infty} a_n J_n(k_\varepsilon \rho)\, e^{jn\phi},$$

$$E_\rho^c(\rho,\phi) = -\frac{\mu\omega}{k_\varepsilon^2 \rho} \sum_{n=-\infty}^{+\infty} a_n n J_n(k_\varepsilon \rho)\, e^{jn\phi}$$

$$= -\frac{Z_0}{\varepsilon_{\mathrm{rc}}\,(2\pi/\lambda)} \frac{1}{\rho} \sum_{n=-\infty}^{+\infty} a_n n J_n(k_\varepsilon \rho)\, e^{jn\phi}, \quad (7)$$

$$E_\phi^c(\rho,\phi) = -j\frac{\mu\omega}{k_\varepsilon^2} \sum_{n=-\infty}^{+\infty} a_n \frac{\partial}{\partial\rho}\psi_n$$

$$= -j\frac{Z_0}{\sqrt{\varepsilon_{\mathrm{rc}}}} \sum_{n=-\infty}^{+\infty} a_n J_n'(k_\varepsilon \rho)\, e^{jn\phi}.$$

In the equations above k_ε is the propagation constant of the cylindrical material, given by $k_\varepsilon = (2\pi/\lambda)\sqrt{\varepsilon_r - j(\sigma/\omega\varepsilon_0)} = (2\pi/\lambda)\sqrt{\varepsilon_{\mathrm{rc}}}$, where σ is conductivity and ε_r is relative dielectric constant.

The details for the evaluation of the coefficients a_n are given in Appendix B, where the following equations for the electric field inside the dielectric cylinder are established:

$$E_\rho^c(\rho,\phi) = \sum_{n=-\infty}^{+\infty} E_{\rho n}^c(\rho,\phi);$$

$$E_\phi^c(\rho,\phi) = \sum_{n=-\infty}^{+\infty} E_{\phi n}^c(\rho,\phi). \quad (8)$$

The distribution of the power loss density (PLD) is the plot of the SAR multiplied by the mass density of the medium. The PLD in the medium is evaluated by

$$\mathrm{PLD}(\rho,\phi) = \frac{\sigma}{2}\left[\left|\sum_{n=-\infty}^{\infty} E_{\rho n}^c(\rho,\phi)\right|^2 + \left|\sum_{n=-\infty}^{\infty} E_{\phi n}^c(\rho,\phi)\right|^2\right]. \quad (9)$$

Given the ID of the Petri dish (34 mm), it is worth noting that at 1 GHz $ka = 0.366$, so relatively few harmonics have an amplitude of relevance ($n \approx$ 3-4). At 5 GHz, $ka = 1.83$, so a large number of harmonics ($n \approx$ 20–30) enter into the computation of the PLD. Note that the PLD is symmetric with respect to the ϕ coordinate, as expected.

Now, let us compare the results from (9) with the computations using a FDTD approach. Figure 5 shows the PLD at 0.2 mm from the bottom of a 34 mm ID Petri dish containing 4 mL of medium at 3, 4, and 5 GHz. A plane wave with electric field amplitude of 100 V/m is incident from the x direction. The PLD was computed using the commercial software CST Microwave Studio 2010 considering a 34 mm ID Petri dish of Perspex with 0.5 mm wall thickness (i.e., a 35 mm outside dish diameter) filled with 4 mL of Dulbecco's modified Eagle's medium (DMEM). The model takes into account the presence of the meniscus. The analysis domain is a cubic box, 40 cm on the side, filled with air. The electric properties of the culture medium are $\varepsilon_r = 42$ and $\sigma = 1.6$ S/m and those of the sample holder are $\varepsilon_r = 2.6$ and $\sigma = 0$ S/m. These values were used for all frequencies and both computational methods.

For each frequency, the module was solved with radiation boundary conditions and mesh of 20 lines per wavelength, resulting in more than 3×10^6 mesh cells.

Figure 6 plots the PLD patterns in an infinite (in the axial direction) cylindrical column of liquid having the same dielectric characteristics and diameter as the medium in the Petri dish of Figure 5, using the analytic method of (9). The plane wave is H-polarized in the direction of the cylindrical axis and is incident from the same direction as in Figure 5.

Comparing the plots in Figures 5 and 6, it is clear that the infinite cylindrical model gives results that are more similar to the FDTD computations with increasing frequency, as expected when a larger number of harmonics enter the calculation. The analytical results present sharper contours of the cylindrical stationary waves boundaries because of the absence of voxel meshing and of smoothing that occurs because of field scattering from the boundaries of a liquid of short height. Notably, despite the absence of meshing and scattering, the infinite model correctly predicts the radii of curvature of the stationary cylindrical waves and the progress from single to double focusing of the incident energy. As both calculations show, at 5 GHz, a 34 mm ID Petri dish with 4 mL medium acts as a dual focus lens delivering a highly nonuniform exposure to a cell preparation at the bottom of the vessel. An almost identical pattern would be obtained by a dissipative dielectric antenna of the same diameter and infinite axial length. This last example clearly illustrates that the medium acts as a receiving antenna that delivers the incident EM energy to the biological cells at the bottom of a Petri dish in a pattern depending only on the geometry, frequency, and the dielectric characteristics of the liquid. The living cells under test are a passive load of the receiving antenna, albeit being a load of very small mass.

4. Conclusion

This paper has shown that the details of the geometry of the medium inside a Petri dish or a test tube are extremely important to the determination of the SAR or the PLD in the vessel. Based on these facts, it should be clear that the medium acts as a dielectric receiving antenna for the incident electromagnetic energy to which the living cells are exposed. At frequencies below 2 GHz, depending on polarization and wavelength, the liquids in Petri dishes and test tubes behave as a loop antenna or a dielectric waveguide, which in fact is just another type of antenna. The PLD patterns in a shallow liquid (few mm in depth) contained in a relatively wide dish can be modeled with good approximation as an infinitely long dissipative cylindrical antenna with a diameter equal to the ID of the vessel, provided that the liquid depth is more than $\lambda/30$. Viewing the medium as the antenna of the biological preparations has important ramifications for the results of in vitro experiments using different vessels. The same incident

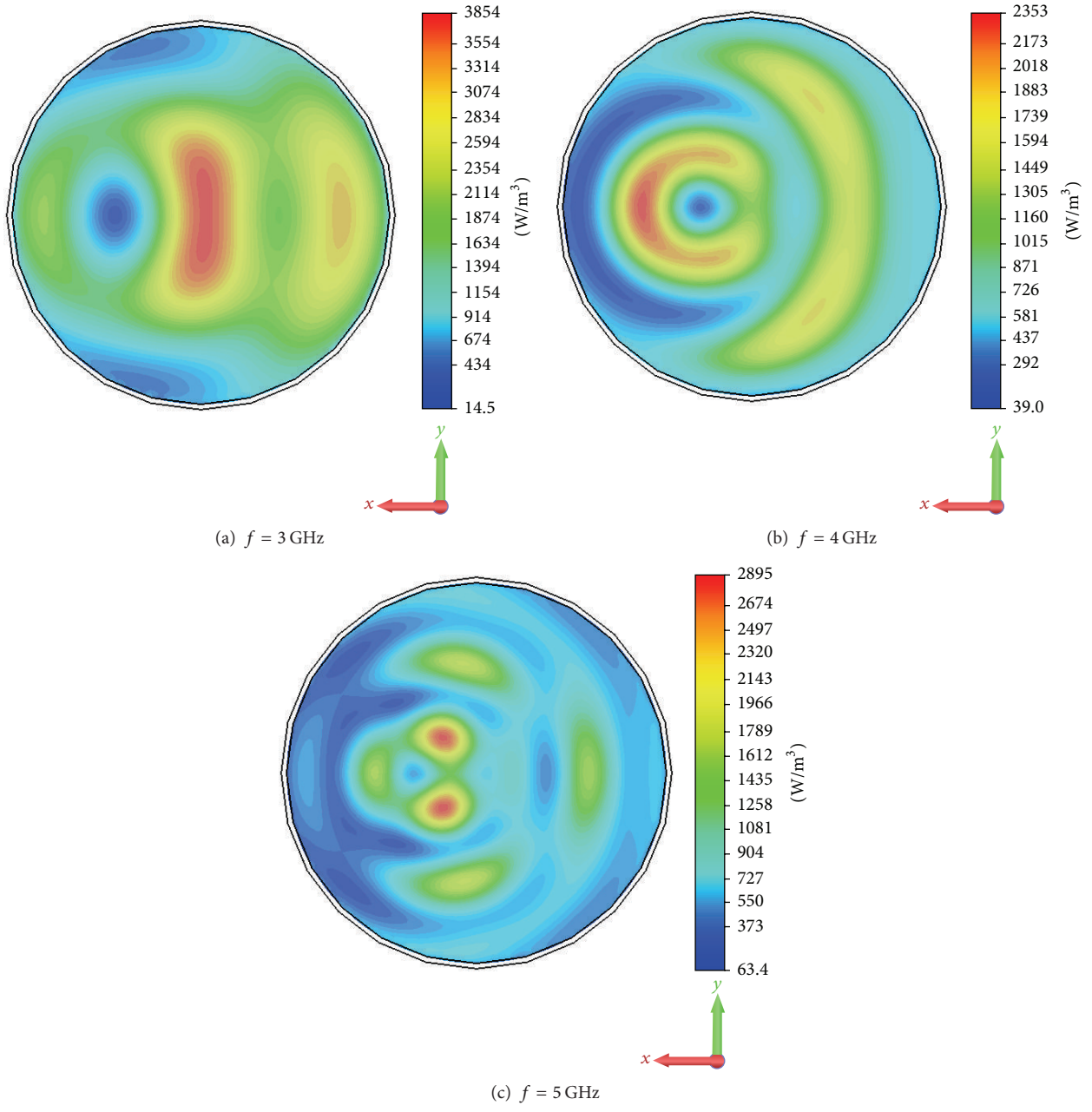

Figure 5: PLD versus frequency at 0.2 mm from the bottom of a 35 mm Petri dish (FDTD).

EM fields may result in very different exposure patterns to the test cells or tissues depending on the dielectric characteristics of the medium, its geometry (shape and size), and the material of the vessel walls (which affect the meniscus shape). Obviously, different spatial power absorption may cause different biological outcomes for in vitro experiments.

Finally, the analytic methods presented here may be valuable to research biologists for evaluating the behavior of the medium as an antenna for fast, preliminary selection of the best vessels for the intended research, using widely available computational tools, if FDTD software and computational power are not accessible. In future efforts, the present analytical model (an infinitely long cylinder of dissipative dielectric) for the medium of a biological preparation exposed in a Petri dish will be refined to a liquid disk of finite height. Such a model could be used as a canonical model for testing FDTD computations. The antenna models and methods presented are not intended to replace the use of numerical algorithms for the accurate evaluation of the EM exposure of biopreparations, but they can be used for a quick, preliminary evaluation of an exposure system and as validation of FDTD computations.

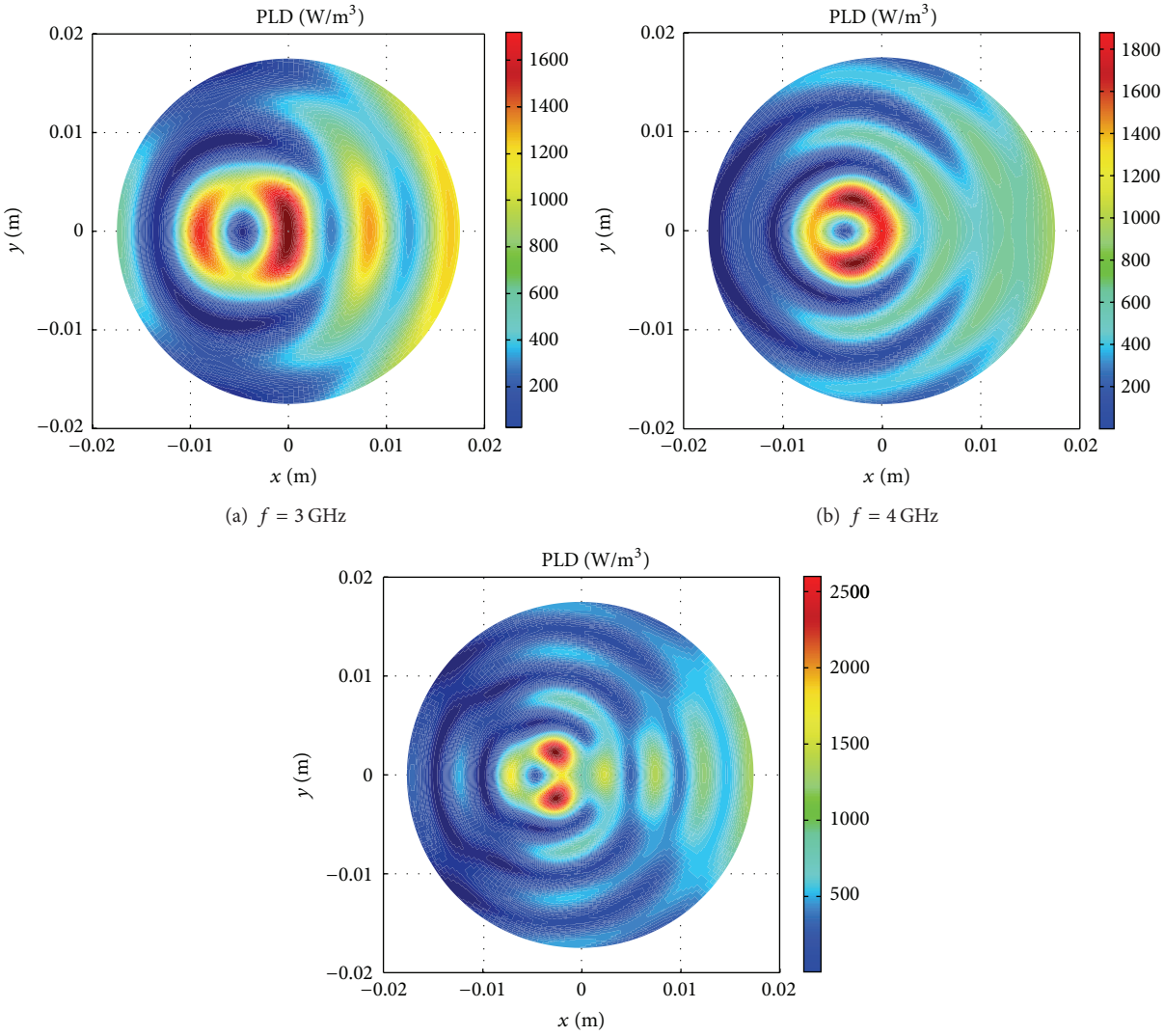

FIGURE 6: PLD versus frequency in an infinite cylindrical liquid column exposed to a plane wave (analytic method).

Appendices

A. *E*-Field at the Bottom of a Petri Dish from Faraday's Law

Faraday's theorem is applied systematically to all the possible paths through the meniscus that pass through the bottom of the dish, thus forming a three-dimensional loop antenna. As shown in Figure 7 for the central cross section of a Petri dish, there is a double infinity of loops that contribute to the 1,800 MHz *E*-field induced at the bottom of the dish.

It is worth noticing that the contribution to the line integral of the induced *E*-field along a semicircular path L of radius D within the meniscus can be evaluated by the following equation:

$$\int_L \vec{E} \cdot \overrightarrow{dl} = \int_0^{\pi} E(\theta) \sin\theta R_d d\theta = E_{\text{ave}} \times D. \quad \text{(A.1)}$$

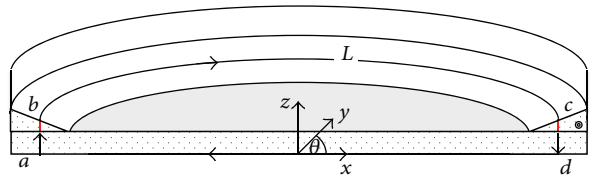

FIGURE 7: Faraday paths in the meniscus forming loops along the bottom of the dish.

The net effect of all the paths can be summed by considering that the meniscus geometry is well approximated by a triangle as shown in Figure 8. The *E*-field acts similarly to a gravity force over the cross section of the meniscus. The highest number (density) of paths is at the edge of the meniscus and their number tapers linearly in the direction of the center of the dish. All the "weights" (contributions) of the various paths

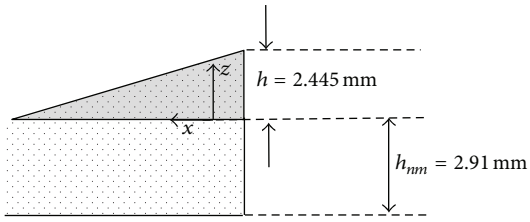

Figure 8: Details of approximate meniscus geometry.

can be collapsed at the "center of gravity" of the meniscus cross section exactly like any distributed mechanical force. Using (A.1), it is possible to write the expression for the average electric field in the close path crossing the bottom of the dish, up into the meniscus, around the meniscus, and back down to the bottom of the dish as shown in Figure 7. If $D(x)$ denotes the path diameter and $h_p(x,z)$ the height of the integration path (see Figure 8), the equation for the average E intensity at the bottom of the dish is

$$E(x,z) = \omega\mu H \frac{h_p(x,z)\, D(x)}{\left[2h_p(x,z) + 2D(x)\right]}. \tag{A.2}$$

In the previous equation $h_p(x,z)$ is given by $h_{nm}+z$, as shown in Figure 8.

The equations for the "center of gravity" coordinates are

$$X_c = \frac{\iint_A E(x,z)\, x\, dx\, dz}{\iint_A E(x,z)\, dx\, dz} = 16.18\,\text{mm},$$
$$Z_c = \frac{\iint_A E(x,z)\, z\, dx\, dz}{\iint_A E(x,z)\, dx\, dz} = h_{nm} + 1.1\,\text{mm}. \tag{A.3}$$

In the above equations, the domain of integration A is the cross sectional area of the meniscus and h_{nm} is the height of the liquid in the middle of the dish as shown in Figure 8.

The average value of the field E_{AV} along the bottom of dish is then

$$E_{\text{AV}} = X_c \frac{(Z_c + h_{nm})}{\left[2X_2 + (h_{nm} + Z_c)\right]}. \tag{A.4}$$

B. Calculation of the Coefficients of the E-Field Series

The boundary conditions for the axial magnetic field and the ϕ component of the electric field require their continuity at the dielectric cylindrical surface: there the scattered fields must be equal to the sum of the incident and the transmitted field into the cylinder for $\rho = a$. For each harmonic of the field it must be

$$H_0 j^{-n} J_n(ka) + a_n J_n(k_\varepsilon a) = j^{-n} b_n H_n^{(2)}(ka),$$
$$\frac{kH_0}{\omega\varepsilon_0} j^{-n} J_n'(ka) - j\frac{\mu\omega}{k_\varepsilon} a_n J_n'(k_\varepsilon a) = \frac{k}{j\omega\varepsilon_0} j^{-n} b_n H_n'^{(2)}(ka). \tag{B.1}$$

Equations (B.1) can be recast in the form

$$H_0 \frac{J_n(ka)}{H_n^{(2)}(ka)} + j^n a_n \frac{J_n(k_\varepsilon a)}{H_n^{(2)}(ka)} = b_n, \tag{B.2}$$

$$jH_0 \frac{J_n'(ka)}{H_n'^{(2)}(ka)} + \frac{j^n}{\sqrt{\varepsilon_{\text{rc}}}} a_n \frac{J_n'(k_\varepsilon a)}{H_n'^{(2)}(ka)} = b_n. \tag{B.3}$$

Subtracting (B.2) from (B.3), we find

$$H_0 \left[\frac{J_n(ka)}{H_n^{(2)}(ka)} - \frac{J_n'(ka)}{H_n'^{(2)}(ka)}\right] + j^n a_n \left[\frac{J_n(k_\varepsilon a)}{H_n^{(2)}(ka)} - \frac{1}{\sqrt{\varepsilon_{\text{rc}}}} \frac{J_n'(k_\varepsilon a)}{H_n'^{(2)}(ka)}\right] = 0. \tag{B.4}$$

From (B.4) the a_n terms are promptly established:

$$a_n = -j^{-n} H_0 \cdot \frac{\left[J_n(ka)/H_n^{(2)}(ka) - J_n'(ka)/H_n'^{(2)}(ka)\right]}{\left[\left(1/\sqrt{\varepsilon_{\text{rc}}}\right)\left(J_n'(k_\varepsilon a)/H_n'^{(2)}(ka)\right) - J_n(k_\varepsilon a)/H_n^{(2)}(ka)\right]}. \tag{B.5}$$

We are not interested in computing the scattered fields, so the b_n terms need not be evaluated. From (B.5), given the parity of the ratios ($R_n = R_{-n}$) of the Bessel functions, only the a_n with positive and zero index need to be computed. The electric field components in the dielectric can be expressed as

$$E_\rho^c(\rho,\phi) = -\frac{Z_0}{\varepsilon_{\text{rc}}(2\pi/\lambda)} \frac{1}{\rho} \sum_{n=-\infty}^{+\infty} a_n n J_n(k_\varepsilon \rho)\, e^{jn\phi},$$
$$E_\phi^c(\rho,\phi) = -j\frac{Z_0}{\sqrt{\varepsilon_{\text{rc}}}} \sum_{n=-\infty}^{+\infty} a_n J_n'(k_\varepsilon \rho)\, e^{jn\phi}. \tag{B.6}$$

Conflict of Interests

The authors declare that there is no conflict of interests regarding the publication of this paper.

References

[1] F. Apollonio, M. Liberti, A. Paffi et al., "Feasibility for microwaves energy to affect biological systems via nonthermal mechanisms: a systematic approach," *IEEE Transactions on Microwave Theory and Techniques*, vol. 61, no. 5, pp. 2031–2045, 2013.

[2] A. W. Guy, C.-K. Chou, and J. A. McDougall, "A quarter century of in vitro research: a new look at exposure methods," *Bioelectromagnetics*, vol. 20, no. 8, p. 522, 1999.

[3] J. Schuderer, T. Schmid, G. Urban, T. Samaras, and N. Kuster, "Novel high-resolution temperature probe for radiofrequency dosimetry," *Physics in Medicine and Biology*, vol. 49, no. 6, pp. N83–N92, 2004.

[4] J. Schuderer and N. Kuster, "Effect of the meniscus at the solid/liquid interface on the SAR distribution in Petri dishes and flasks," *Bioelectromagnetics*, vol. 24, no. 2, pp. 103–108, 2003.

[5] A. Paffi, F. Apollonio, G. A. Lovisolo et al., "Considerations for developing an RF exposure system: a review for in vitro biological experiments," *IEEE Transactions on Microwave Theory and Techniques*, vol. 58, no. 10, pp. 2702–2714, 2010.

[6] A. Taflove and S. C. Hagness, *Computational Electrodynamics: The Finite-Difference Time-Domain Method*, Artech House, Norwood, Mass, USA, 2005.

[7] A. El Ouardi, J. Streckert, A. Bitz, S. Münkner, J. Engel, and V. Hansen, "New fin-line devices for radiofrequency exposure of small biological samples in vitro allowing whole-cell patch clamp recordings," *Bioelectromagnetics*, vol. 32, no. 2, pp. 102–112, 2011.

[8] L. Laval, P. Leveque, and B. Jecko, "A new in vitro exposure device for the mobile frequency of 900 MHz," *Bioelectromagnetics*, vol. 21, no. 4, pp. 255–263, 2000.

[9] A. Paffi, M. Liberti, V. Lopresto et al., "A wire patch cell exposure system for in vitro experiments at wi-fi frequencies," *IEEE Transactions on Microwave Theory and Techniques*, vol. 58, no. 12, pp. 4086–4093, 2010.

[10] T. Iyama, H. Ebara, Y. Tarusawa et al., "Large scale in vitro experiment system for 2 GHz exposure," *Bioelectromagnetics*, vol. 25, no. 8, pp. 599–606, 2004.

[11] Q. Balzano, V. Hodzic, R. W. Gammon, and C. C. Davis, "A doubly resonant cavity for detection of RF demodulation by living cells," *Bioelectromagnetics*, vol. 29, no. 2, pp. 81–91, 2008.

[12] L. Ardoino, V. Lopresto, S. Mancini, R. Pinto, and G. A. Lovisolo, "1800 MHz in vitro exposure device for experimental studies on the effects of mobile communication systems," *Radiation Protection Dosimetry*, vol. 112, no. 3, pp. 419–428, 2004.

[13] D. Hondros and P. Debye, "Elektromagnetische Wellen an dielektrischen Drähten," *Annalen der Physik*, vol. 337, no. 8, pp. 465–476, 1910.

[14] W. M. Elsasser, "Attenuation in a dielectric circular rod," *Journal of Applied Physics*, vol. 20, no. 12, pp. 1193–1196, 1949.

[15] D. G. Kiely, *Dielectric Aerials*, Methuen & Co., London, UK, 1953.

[16] R. E. Collin, *Field Theory of Guided Waves*, section 11.6, McGraw-Hill, 1960.

[17] J. A. Stratton, *Electromagnetic Theory*, chapter 6, section 6.6, McGraw-Hill Book Company, Inc., New York, NY, USA, 1941.

[18] R. F. Harrington, *Time Harmonic Electromagnetic Fields*, Scattering by Cylinders, chapter 5, section 5–9, McGraw-Hill, New York, NY, USA, 1961.

[19] CST Computer Simulation Technology AG., http://www.cst.com.

[20] A. Bijamov, A. Razmadze, L. Shoshiashvili et al., "Advanced electro-thermal analysis for the assessment of human exposure in the near-field of EM sources," in *Proceedings of the 8th International Conference on Electromagnetics in Advanced Applications (ICEAA '03)*, Paper no. 277, pp. 61–64, Torino, Italy, September 2003.

[21] J.-Y. Chung and C.-C. Chen, "Two-layer dielectric rod antenna," *IEEE Transactions on Antennas and Propagation*, vol. 56, no. 6, pp. 1541–1547, 2008.

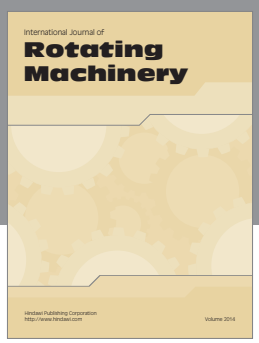

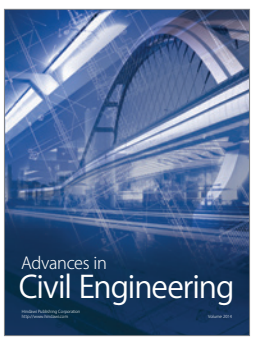

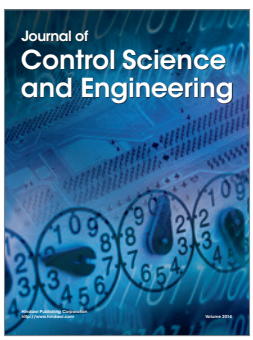

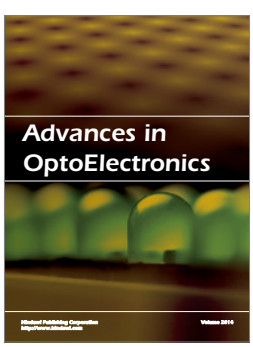

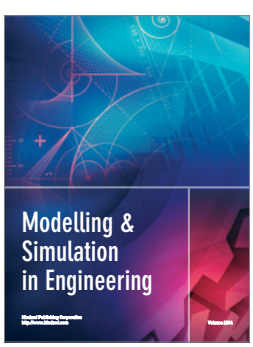

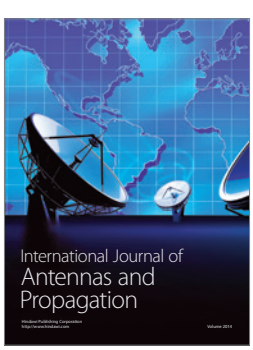

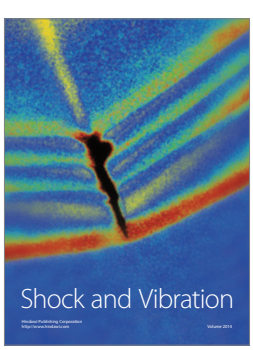

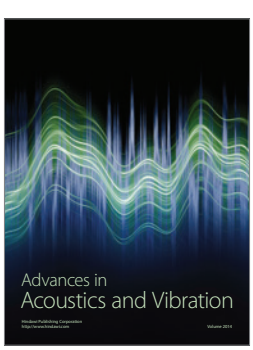

Hindawi

Submit your manuscripts at
http://www.hindawi.com